Red Line Diffuse-Like Aurora Driven by Time Domain Structures Associated with Braking Magnetotail Flow Bursts

Yangyang Shen[1], Jun Liang[2], Anton Artemyev[1,3], Vassilis Angelopoulos[1], Qianli Ma[4,5], Larry Lyons[4], Jiang Liu[1], Yukitoshi Nishimura[5], Xiao-Jia Zhang[6], Ivan Vasko[6], Donald L Hampton[7]

[1]Department of Earth, Planetary, and Space Sciences, University of California, Los Angeles, CA, USA
[2]Department of Physics and Astronomy, University of Calgary, Calgary, AB, Canada
[3]Space Research Institute of Russian Academy of Sciences, Russia, Moscow
[4]Department of Atmospheric and Oceanic Sciences, University of California, Los Angeles, CA, USA
[5]Center for Space Physics, Boston University, Boston, MA, USA
[6]William B. Hanson Center for Space Sciences, University of Texas at Dallas, Richardson, TX, USA
[7]Geophysical Institute, University of Alaska Fairbanks at Fairbanks, Fairbanks, AK, USA

Key Points:

- Predominantly red-line auroras are linked to flow bursts, TDSs, and <1 keV electron precipitation
- For the first time, red-line diffuse-like auroras have been forward-modeled using TREx-ATM with TDS inputs
- A good correlation between forward-modeled and observed red-line emissions suggests that TDSs are a major driver

Corresponding author: Yangyang Shen, yshen@epss.ucla.edu

Abstract

Magnetotail earthward-propagating fast plasma flows provide important pathways for magnetosphere-ionosphere coupling. This study reexamines a flow-related red-line diffuse-like aurora event previously reported by Liang et al. (2011), utilizing THEMIS and ground-based auroral observations from Poker Flat. We find that time domain structures (TDSs) within the flow bursts efficiently drive electron precipitation below a few keV, aligning with predominantly red-line auroral intensifications in this non-substorm event. The diffuse-like auroras sometimes coexisted with or potentially evolved from discrete forms. We forward model red-line diffuse-like auroras due to TDS-driven precipitation, employing the time-dependent TREx-ATM auroral transport code. The good correlation ($\sim$0.77) between our modeled and observed red line emissions underscores that TDSs are a primary driver of the red-line diffuse-like auroras, though whistler-mode wave contributions are needed to fully explain the most intense red-line emissions.

Plain Language Summary

Fast plasma flows in the magnetotail, traveling earthward at several hundred kilometers per second, transport energetic particles and magnetic flux into the inner magnetosphere. Upon braking near Earth's high magnetic flux regions, they trigger plasma instabilities and waves, leading to increased electric currents and particle precipitation in the polar regions. This precipitation, depending on its driver, results in either diffuse-like auroras from electron pitch-angle scattering, or discrete auroras from field-aligned electron acceleration and currents. Our case study highlights the important role of time-domain structures in diffuse-like aurora generation during flow braking. This reveals a new aspect of magnetosphere-ionosphere coupling: the generation of diffuse-like auroras through electron scattering by time-domain structures in braking flow bursts.

1 Introduction

Since their discovery in the 1970's (Scarf et al., 1974; Gurnett et al., 1976), broadband electrostatic noise in the frequency range of tens of Hz up to several kHz have been observed to be ubiquitous in various space plasmas (Ergun et al., 1998; Cattell et al., 2005; Williams et al., 2006). These fluctuations, when examined in the time domain (Matsumoto et al., 1994), manifest unique localized electrostatic solitary structures, comprising mostly electron phase-space holes and double layers, which are collectively termed as time-domain structures (TDSs) (Mozer et al., 2015).

Recently, there have been active discussions on the role of TDS-induced electron scattering in generating diffuse auroras (Mozer et al., 2018; Nishimura et al., 2018; Vasko et al., 2017, 2018; Shen et al., 2020, 2021). While Mozer et al. (2018) proposed that TDSs contribute to electron precipitation into pulsating auroras, Nishimura et al. (2018) argued that TDSs were more likely linked to discrete auroras or non-pulsating diffuse auroras. Furthermore, a few studies showed that TDSs can efficiently scatter less than a few keV electrons into the loss cone, thereby contributing to the diffuse auroral precipitation (Vasko et al., 2017, 2018; Shen et al., 2020, 2021). Although individual conjunction events have revealed moderate correlations between TDSs and diffuse auroras (see Supporting Information in Shen et al., 2020), and their similar statistical distributions in the nightside plasma sheet lend support(Newell et al., 2009; Malaspina et al., 2015), direct evidence remains elusive.

Prior statistical studies revealed that TDSs are abundant in the plasma sheet within most plasma injections and braking fast ion flows or bursty bulk flows (BBFs) (Gurnett & Frank, 1977; Angelopoulos et al., 1992; Ergun et al., 2015; Malaspina et al., 2015). These fast ion flows often manifest in the ionosphere as north–south auroral structures or "stream-

ers" (e.g., Lyons et al., 2012; Henderson, 2012; Nishimura et al., 2011). Auroral streamers are typically discrete in nature and are linked to upward field-aligned currents forming on the western edge of flow bursts (Nakamura et al., 2001; Nishimura et al., 2011). However, some streamers may coexist with or evolve into diffuse-like aurora enhancements as they move equatorward and reach the inner edge of the plasma sheet (Henderson et al., 1998). Within the braking flows, TDSs may contribute to electron precipitation into structured diffuse-like and non-accelerated auroras (Sergeev et al., 2004; Shen et al., 2020).

Low-energy (<∼1 keV) electron precipitation more effectively excites red-line (630 nm) auroras, whereas higher-energy (>1 keV) electrons predominantly induce green-line (557.7 nm) and blue-line (427.8 nm) auroras. Thus, TDSs are likely linked to red-line-dominated auroras, especially when the plasma sheet state is prime for such low-energy precipitation, like quiet times with low temperatures. In fact, to reliably identify TDS-driven diffuse auroras, non-substorm conditions are more suitable, as it is often challenging to disentangle aggregated effects from different, concurrent drivers during substorms that preclude direct linkage to flow bursts and TDSs (e.g., Sergeev et al., 2012; Shen et al., 2023).

One potential example has been reported by Liang et al. (2011), where conjugate THEMIS and ground-based optical and radar observations revealed flow-related auroral signatures, including high-latitude poleward boundary intensifications (PBIs), streamer-like discrete auroras, and red-line diffuse-like auroras that are associated with the discrete forms. In that study, THEMIS waveform data and potential TDS signatures have not been investigated, leaving the impact of TDS-induced electron scattering on red-line auroras unresolved. In this paper, we revisit this event, aiming to provide the first forward modeling and data-model comparison of red-line diffuse auroras driven by TDSs.

2 Instrumentation and Models

We use the following data from THEMIS (Angelopoulos, 2008): electron and ion fluxes and moments measured by the Electrostatic Analyzers (ESA) and the Solid State Telecope (SST) instruments in the energy range of several eV up to 900 keV (McFadden et al., 2008; Angelopoulos et al., 2008), DC vector magnetic fields at spin resolution (∼3 s) measured by the Fluxgate Magnetometers (FGM) (Auster et al., 2008), electric and magnetic field wave power spectra within 1 Hz–4 kHz (FBK with 6 frequency bands and FFP with 64 bands), and waveform data at 8,192 samples per second (sps, DC-coupled), measured by the Electric Field Instrument (EFI), the search coil magnetometer (SCM), and the Digital Fields Board (DFB) (Le Contel et al., 2008; Bonnell et al., 2008; Cully et al., 2008).

The flow-related red-line auroral event occurred during 10:30–11:30 UT on March 3, 2009. Following Liang et al. (2011), we primarily use the ground-based Poker Flat meridian spectrograph (PFMSP) for auroral observations, recording every 15 seconds and capturing emissions in the red (630 nm), green (557.7 nm), blue (427.8 nm), and proton H_β (486.1 nm) lines along the meridian. Complementarily, the Poker Flat digital all-sky camera (DASC) provided 2D auroral data to elucidate the longitudinal or magnetic local time (MLT) extent of the red-line diffuse auroras. Note that the DASC does not provide absolute intensities of 630 nm emissions and it recorded images at 41-s cadence for this event. We also use auroral observations from the THEMIS whitelight all-sky imager (ASI) at Fort Yukon with 3-s cadence (Mende et al., 2008).

Although TDSs include different types of nonlinear electrostatic structures as noted by Mozer et al. (2015), electron phase space holes are the predominant type in the near-Earth plasma sheet (e.g., Ergun et al., 2015; Malaspina et al., 2018). Electron scattering by electron holes can be quantified using the quasi-linear approach initially devel-

oped for an ensemble of plane waves (Kennel & Engelmann, 1966; Lyons, 1974). We use the formulation of local pitch-angle diffusion coefficients $D_{\alpha\alpha}$ derived in Vasko et al. (2018) and refined by Shen et al. (2021). We bounce average the local diffusion rates using the standard procedure (Lyons et al., 1972; Glauert & Horne, 2005):

$$\langle D_{\alpha_{eq}\alpha_{eq}} \rangle = v^{-1}\tau_B^{-1} \int D_{\alpha\alpha} \left(\partial\alpha_{eq}/\partial\alpha\right)^2 \left(\partial s/\partial\lambda\right) d\lambda/\cos\alpha, \tag{1}$$

where the integration is over the period of bounce motion τ_B, and $s = s(\lambda)$ is the length of a field line. We use the relatively realistic T89 magnetic field model for bounce-averaging (Tsyganenko, 1989; Ma et al., 2012). The latitudinal profile of **B** near the equator is adjusted to reduce stretching so as to align with local THEMIS magnetic field observations (e.g., Ni et al., 2012). In addition, bounce-averaged pitch angle diffusion coefficients due to transient whistler-mode waves are also calculated using the Full Diffusion Code (Ni et al., 2008; Ma et al., 2020), including the Landau (n=0) and higher order (n up to $\pm$10) cyclotron harmonic resonances.

We use the full precipitating electron distributions calculated from quasilinear diffusion theory to forward model TDS-driven red-line auroras. Because the varying timescale of precipitation is typically shorter than the radiative timescale (~110 s) of 630 nm emission, it is imperative to use a time-dependent auroral transport code, such as the TREx-ATM model (Liang et al., 2016). TREx-ATM is a time-dependent ionosphere aurora model, adopting the two-stream electron transport code embedded in the GLOW model (Solomon et al., 1988) and ambipolar diffusion to compute the electron transport in the atmosphere, with additional capabilities to compute the impact ionization, secondary electron production, and impact excitation of neutrals.

3 Results

The event featuring bursty bulk flows and red-line auroras was observed from 11:40 to 11:20 UT on March 3, 2009. During this time, THEMIS-C spacecraft detected a series of high-speed flow bursts (>400 km/s) in the Earth's plasma sheet, as shown in Figure 1. Figures 1a–1c illustrate the magnetic fields threading all five THEMIS spacecraft, modeled by T89, alongside the 2D ionospheric red-line auroras observed by Poker Flat DASC. The red-line auroras spanned nearly 45° in magnetic longitude or 3 hrs in MLT, primarily drifted eastward, occasionally moving equatorward, and exhibited both diffuse-like and discrete enhancements.

For this event complementary ground-based measurements, including THEMIS ASIs and Poker Flat incoherent scatter radar, provided synergistic auroral and ionospheric density observations as detailed by Liang et al. (2011). While not described again here, the key findings include: (1) flow-related auroras featured intermittent poleward boundary intensifications (PBIs) and streamer-like green line emissions, occasionally coinciding with or transitioning to predominantly red-line diffuse-like auroras at lower latitudes; (2) ionospheric density altitude profiles were consistent with the red-line emissions and soft (<1 keV) electron precipitation; (3) southward-moving density patches corresponded to earthward flow bursts and red-line auroral enhancements. It was noted that the absence of substantial density enhancements above 200 km and the latitudinally-extended red-line diffuse-like emissions were inconsistent with typical small-scale Alfvénic auroras and broadband acceleration (Chaston et al., 2003; Liang et al., 2019). However, for some observed discrete auroras, such as the bright stripes around -100° magnetic longitude and discrete structures near the poleward boundary (likely linked to PBIs) in Figure 1c, Alfvénic acceleration cannot be ruled out (Damiano et al., 2015; Tian et al., 2021; Hull et al., 2022), though these aspects are not the main focus of this study. Auroral features will be further examined using multi-spectra PFMSP measurements.

Figures 1b–1c indicate that of the five THEMIS spacecraft, THB and THC were closest to midnight, with their footprints less than 1 hr MLT east of Poker Flat. THC

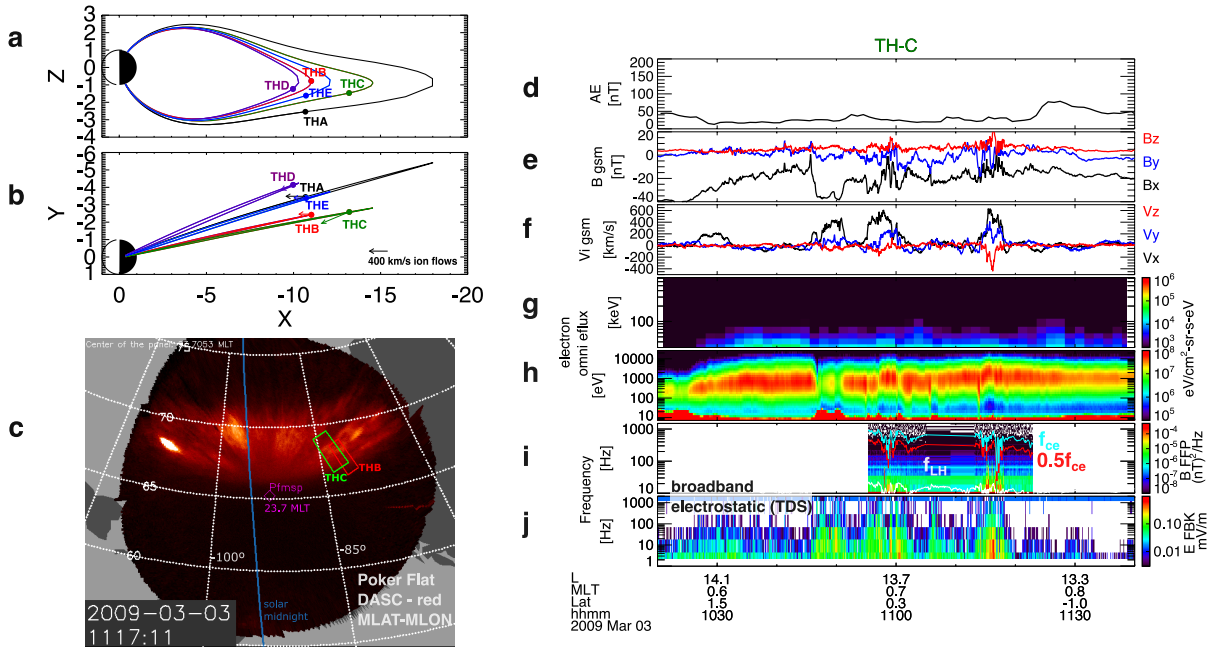

Figure 1. Overview of the flow-related red-line diffuse aurora event observed by THEMIS-C and Poker Flat all-sky camera (DASC). (a–b) Field line configuration threading the five THEMIS spacecraft in the GSM coordinates. Colored vectors represent ion flow velocities for each spacecraft. (c) Poker Flat DASC red-line auroras measured near 11:17 UT. The grids represent AACGM magnetic latitude and magnetic longitude, while the blue line marks the actual local midnight. The assumed emission height and approximate footprints of THEMIS-B (red box), THEMIS-C (green box), and Poker Flat have been mapped to ∼200 km altitude using different Tsyganenko models of T89, T96, and T01. (d) THEMIS AE index. (e) Magnetic fields. (f) Ion flow velocities. (g-h) Electron energy spectrogram from 7 eV up to 900 keV. (i) Magnetic field FFP spectra in 10 Hz–2 kHz. (j) Electric field FBK spectra up to 2 kHz.

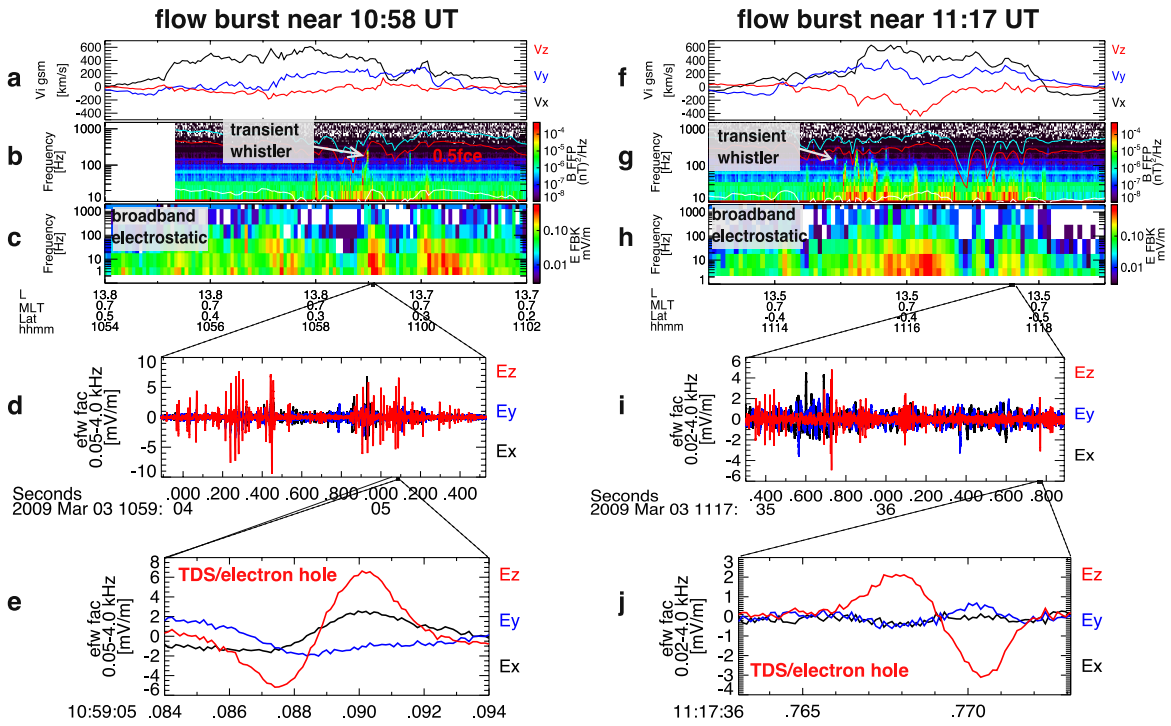

Figure 2. Zoomed-in view of the plasma waves within the two flow bursts near 10:58 UT (a–e) and 11:17 UT (f–j). Panels from top to bottom are: ion flow velocities, FFP magnetic field spectra, FBK electric field spectra, waveform measurements of high-frequency (>20 Hz and >50 Hz) electric fields in the field-aligned coordinates (**B** is in the z direction), and expanded views of milisecond-scale electron phase-space holes, also known as time-domain structures (TDSs).

detected all flow bursts exceeding 400 km/s within BBFs, whereas THB, positioned further earthward, registered only a weaker flow burst (∼200 km/s) that had waned during inward propagation. Figure 1d shows that the *AE* index remained below 80 nT throughout the event. Three strong flow bursts were recorded between 10:40 and 11:20 UT, each lasting ∼5 minutes. The latter two, occurring closer to the equator, were accompanied by $|B_x|$ decreases, notable B_z dipolarizations (Figure 1e), and slightly energized electron spectra (Figure 1h). Despite heightened flow activity, the plasma sheet temperature remained below 1 keV (Liang et al., 2011). Figures 1i–1j show that the flow bursts corresponded to enhanced broadband electrostatic fluctuations (or TDSs) with frequencies ranging from tens of Hz to several kHz. Additionally, sporadic electromagnetic wave power enhancements, mostly below ∼20 Hz, indicate the presence of kinetic Alfvén waves (KAWs) (e.g., Chaston et al., 2012; Malaspina et al., 2018; Shen et al., 2023).

Figure 2 provides a detailed view of wave spectra and waveform measurements associated with two flow bursts near 10:58 UT and 11:17 UT. Throughout the flow intervals, there were continuous enhancements in broadband electrostatic fluctuations. Figures 2d, 2e, 2i, and 2j clearly show that these broadband electrostatic fluctuations predominantly consisted of electron phase-space holes, identified by a deficit of the electron phase space density that exhibits bipolar parallel (in the z direction) and unipolar perpendicular (in the x and y direction) electric fields, on the timescales of milisecond or on the spatial scales of the local Debye length (Muschietti et al., 1999; Hutchinson, 2017; Lotekar et al., 2020). In contrast, whistler-mode waves were more ephemeral, characterized by sporadic, narrow-band magnetic power enhancements lasting less than one minute within the flow intervals (Figures 2b and 2g).

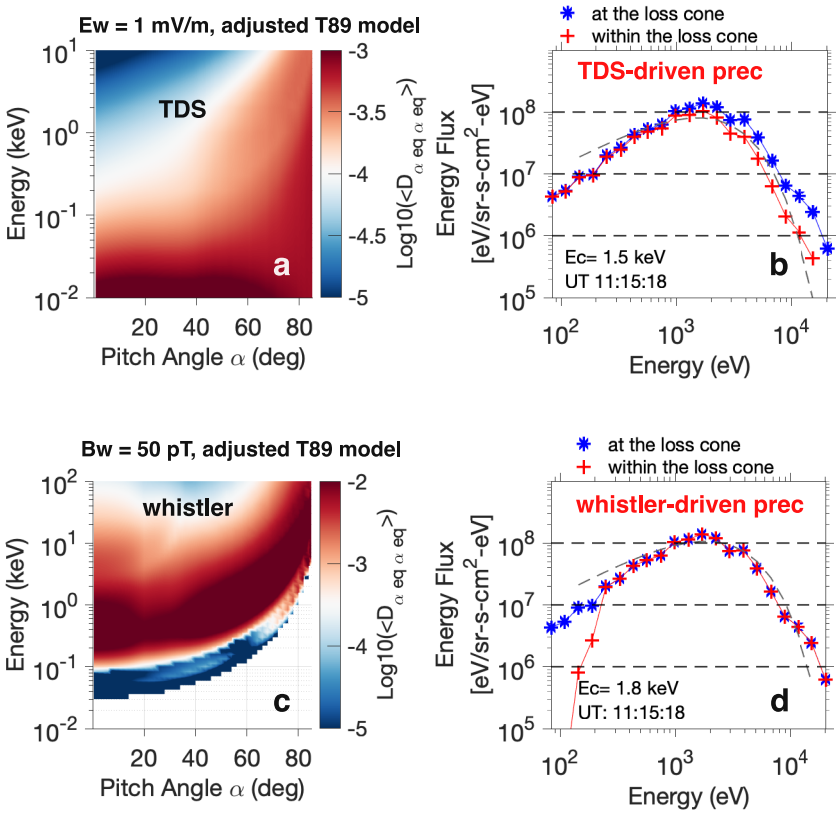

Figure 3. (a, c) TDS- and whistler-driven bounce-averaged electron pitch-angle diffusion rates ($\langle D_{\alpha_{eq}\alpha_{eq}}\rangle$) as a function of energy and pitch angle. We use adjusted T89 model for bounce averaging. (b, d) Example energy flux distributions extrapolated to the loss cone (blue) and calculated within the loss cone (red) based on $\langle D_{\alpha_{eq}\alpha_{eq}}\rangle$. The gray-dashed curves indicate Maxwellian fittings of the precipitating distributions due to TDSs and whistlers, indicating characteristic energies of 1.5 keV and 1.8 keV near 11:15:18 UT.

Based on the observed characteristics of TDSs and whistler-mode waves, we proceed to calculate bounce-averaged electron pitch-angle diffusion rates $\langle D_{\alpha_{eq}\alpha_{eq}}\rangle$ and resulting electron distributions precipitating into the ionosphere (Shen et al., 2021; Ma et al., 2012, 2020). TDSs can be generated locally at various latitudes and continuously along the propagation of flow bursts and injections toward Earth (Ergun et al., 1998; Franz et al., 2005; Mozer et al., 2015; Malaspina et al., 2015). We assume a latitudinal distribution of electron holes to be within ±25° near the equator; increasing the latitude extent to ±45° enhances the diffusion rate near the loss cone by <20%. For transient whistler-mode waves, we determine the average wave spectra near 11:15 UT (Figure 2g) as having a Gaussian with a lower limit ω_1=0.15Ω_{ce}, a mean frequency ω_2=0.3Ω_{ce}, an upper limit ω_m=0.45Ω_{ce}, a semi-bandwidth $\delta\omega$=0.075Ω_{ce}, and a mean wave amplitude B_w=50 pT. No whistler-mode waves were measured by waveform data in our event, thus we do not have direct information on their wave normals. For the nightside equatorial plasma sheet (Li et al., 2011; Agapitov et al., 2013; Meredith et al., 2021), we can assume parallel whistlers confined within ±15° latitude near the equator, having Gaussian wave normals with a width θ_w=10°, a minimum θ_{min}=0°, and a maximum θ_{max}=30°. We set the background n_e ~0.6 cm^{-3}, f_{pe}/f_{ce} ~14.4, and L ~14.0 based on THEMIS observations. For bounce averaging, we use the T89 model with slight adjustments near the equator to align with THEMIS-C local B observations.

Figures 3a and 3c present the calculated $\langle D_{\alpha_{eq}\alpha_{eq}} \rangle$ as a function of energy and pitch angle, resulting from electron scattering by TDSs and whistler-mode waves, respectively. Near the loss cone ($\sim$1°), TDSs efficiently induce pitch-angle scattering at energies below a few keV, with $\langle D_{\alpha_{eq}\alpha_{eq}} \rangle$ on the order of 10^{-4}–10^{-3} s^{-1}, assuming E_w $\sim$1 mV/m. Due to large f_{pe}/f_{ce} for this event, whistler-mode waves can also drive efficient electron scattering at energies as low as 200 eV, but the scattering rates exhibit a broad peak near 1 keV, extending up to 100 keV. This suggests that whistler-mode waves tend to produce more energetic precipitation spectra compared with TDSs.

Example precipitating electron energy distributions are shown in Figures 3b and 3d. The differential energy flux (red pluses) within the loss cone can be estimated as $x(E)J\,(E, \alpha_{LC})$, where

$$x(E) = 2\int_0^1 I_0(Z_0\tau)\tau d\tau / I_0(Z_0), \tag{2}$$

being the index of loss cone filling, $J(E, \alpha_{LC})$ is the electron differential energy flux near the loss cone (blue stars), I_0 is the modified Bessel function with an argument $Z_0 \simeq \alpha_{LC}/\sqrt{\langle D_{\alpha\alpha}\rangle_{LC} \cdot \tau_{loss}}$ (Kennel & Petschek, 1966), and τ_{loss} is assumed to be half of the bounce period.

Time-varying precipitating electron full distributions are input into the time-dependent TREx-ATM code to forward model red-line auroras and compare their evolution with that of the measured red-line diffuse-like auroras by PFMSP. We begin by examining PFMSP auroral observations. Figures 4a–4d display approximately correlated ion flow bursts, TDS E_w, and enhanced auroral activities in the green line (577.7 nm), blue line (427.8 nm), and red line (630 nm). To obtain wave amplitudes of TDSs from FBK spectra (Figure 2), we integrate wave power in the frequency range of 20–900 Hz, as informed by TDS wavelet analyses (Shen et al., 2021). The flow bursts (>400 km/s) were associated with intermittent poleward boundary intensifications (PBIs) near 160° elevation angle (or $\sim$68° magnetic latitudes) in the green and blue line emissions, exhibiting distinct equatorward movement. These features align with auroral streamers associated with earthward flow channels in the plasma sheet (e.g., Lyons et al., 2012; Henderson, 2012; Nishimura et al., 2011).

However, the majority of the auroral enhancements were noted in the red line, predominantly equatorward of the green-line enhancements. These enhanced red-line emissions, characterized by "patchiness" or short-lived activations, coincided with TDS amplitude increases and exhibited discernible equatorward movement. As noted by Liang et al. (2011), this movement was also in accord with the equatorward shift of soft electron precipitation and enhanced density patches at altitudes above 150 km. Figure 4f suggests that TDS-driven precipitation has characteristic energies mostly below 1 keV, consistent with the overwhelmingly red-line emissions and soft electron precipitation. In contrast, assuming the presence of whistler-mode waves throughout the flow bursts near 10:58 UT and 11:17 UT, these would produce precipitation with characteristic energies exceeding 1 keV.

To compare with TREx-ATM model output, we need to identify PFMSP red-linediffuse-like aurora intensifications that were approximately conjugate with THEMIS observations. First, we focus on the time interval between 10:45 and 11:30 UT, during which the longitudinal separation between the PFMSP meridian and projected THEMIS-C footprints was less than 15°, or equivalently $|\Delta MLT|$ <1 hr (Figure 4g). Second, we adjust the PFMSP red-line data counts by subtracting a uniform background attributed to ambient diffuse auroras, likely arising from non-TDS mechanisms like diffuse proton precipitation (e.g., Lyons et al., 2015) as indicated by PFMSP H_β-line emissions. Third, after applying Van Rhijin correction to data counts for aspect angle effects, we identify an optimum range of elevation angles of 139°–146°, which probably corresponded to THEMIS measurements. These optimal angles were determined by searching the maximum cor-

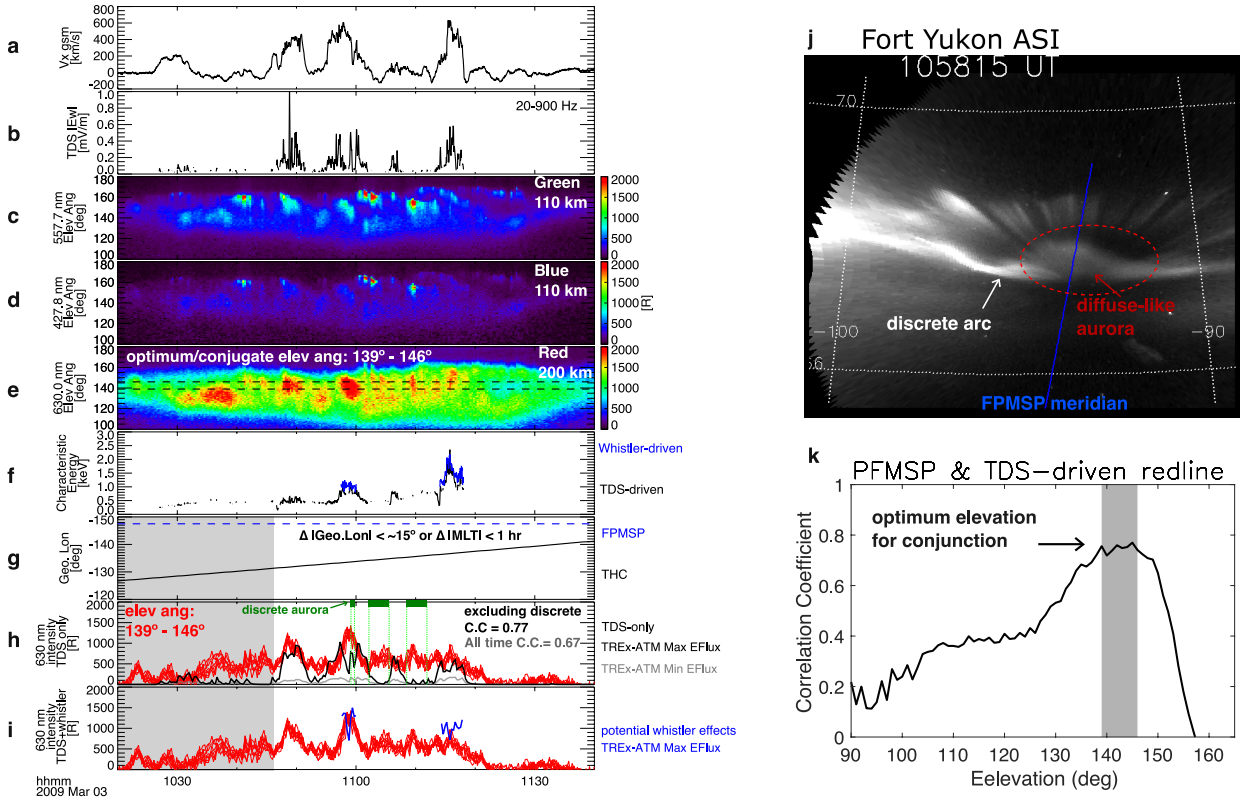

Figure 4. Auroral features and TREx-ATM model results. (a) Ion flow velocity V_x. (b) Root-mean-square TDS electric field amplitudes $|E_w|$ (20-900 Hz). (c-e) PFMSP 557.7-nm green-line, 427.8-nm blue-line, and 630-nm red-line intensity; dashed lines mark optimal elevation angle range for THEMIS conjunction. (f) Characteristic energies of electrons precipitated by TDS (black) and whistler-mode waves (blue). (g) Geographic longitudes of PFMSP and THEMIS-C footprints. (h) 630-nm intensity: PFMSP data (red) vs TDS-driven TREx-ATM model results (black, gray) based on THEMIS maximum and minimum fluxes around the equator (see Supporting Information). (i) TREx-ATM results with additional inputs from assumed, persistent whistler-mode waves; only maximum electron fluxes used. (j) Example ASI whitelight image showing diffuse-like auroras near PFMSP that likely evolved from discrete auroras. (k) Correlation coefficients for PFMSP and TREx-ATM modeled TDS-driven red-line auroras at various elevation angles.

relation coefficients between the modeled and observed red-line emissions across all elevation angles (Figure 4k).

The event exhibited coexisting auroral types due to various mechanisms. TDS-induced soft electron precipitation leads to a broader altitude distribution of both 630 nm and 557.7 nm emissions, unlike the narrow altitude range associated with monoenergetic electron acceleration in discrete arcs. In oblique optical observations, like those from PFMSP and THEMIS ASI, this broader distribution may appear as more "diffusive" auroral forms (see Figure 4j around the PFMSP meridian). Additional ASI auroral images are provided in Supporting Information. The 630-nm emission, particularly sensitive to soft electron precipitation, aligns closely with TDS effects, which we mainly focus on in the study. We have carefully examined the observations from the Fort Yukon ASI (see Supplementary Movie in Liang et al. (2011)) and excluded three periods when discrete arcs predominately contribute to PFMSP red-line emissions.

Figure 4h shows a correlation coefficient of 0.77 between PFMSP observed and TREx-ATM forward-modeled red-line emissions, using inputs solely from TDS-driven precipitation. The TREx-ATM model results, indicated by the black and gray lines, are based on maximum and minimum flux levels measured by THEMIS near the equator during 10:40–11:20 UT. These in-situ measured fluxes were largely controlled by the spacecraft's proximity to the true equator, where $|B_x|$ is minimum (see Supporting Information). Figure 4h reveals that the majority of the observed red-line diffuse-like auroral enhancements during flow bursts can be explained by TDS-driven model results, albeit slightly underestimated for the most intense emissions. Green bars highlight the time intervals of discrete emission peaks, unrelated to TDSs, near 11:00, 11:05, and 11:10 UT. Including these intervals in our analysis lowers the correlation to 0.67. Figure 4i suggests that including potential whistler-mode wave effects along with TDSs in the model offers a better explanation for the two bright red spots near 10:58 UT and 11:17 UT. This implies that whistler-mode waves might also contribute to the most intense red-line diffuse emissions during flow bursts. The compound effects of whistler-mode waves and field-aligned acceleration on energetic electron precipitation obscure TDS's role in 557.7-nm emissions. Nonetheless, we have analyzed TDS-driven TREx-ATM 557.7-nm outputs and observed a weaker correlation with PFMSP's green line ($\sim$0.6).

4 Discussion

Plasma sheet flow bursts are typically linked to ionospheric auroral PBIs and equatorward-moving auroral streamers, as evidenced by white-light all-sky imager (ASI) observations, often around substorm times (Donovan et al., 2008; Nishimura et al., 2011; Forsyth et al., 2020; Yadav et al., 2022). In our non-substorm event, while green-line PBIs and forms resembling equatorward-moving auroral streamers were noted, the most prominent feature was the red-line auroras. These auroras extended towards lower latitudes and often appeared more diffuse than discrete near PFMSP, likely due to wave scattering. Liang et al. (2011) suggests that the predominance of red-line emissions was probably due to a cooler inner plasma sheet (T_e <$\sim$1 keV). Despite strong flows and potential association with hot electrons in the tail leading to streamer-inducing energetic precipitation (Angelopoulos et al., 1992; Nishimura et al., 2020), there was an absence of significant energetic injections intruding the inner plasma sheet around midnight (Figure 1g). This could be attributed to differences in adiabatic motion or Alfvén layers between soft and energetic electrons as they undergo convective, curvature and gradient drifts during inward propagation (e.g., Gabrielse et al., 2017).

While red-line emissions naturally accompany green-line emissions due to the $O(^1S)$ to $O(^1D)$ transition linked with 557.7 nm photo emission (Solomon et al., 1988), the dominance of red-line auroral emissions indicates a major low-energy precipitation population, distinct from the energetic precipitation responsible for green line excitation. This

low-energy precipitation was confirmed by ionospheric density altitude profiles measured by PFISR (Liang et al., 2011). During the event period of our interest, ECH waves were not observed, ruling them out as a cause for the auroral precipitation (Ni et al., 2012; Zhang et al., 2015). Our investigations, encompassing wave spectra and waveform analyses, quasilinear calculations, and aurora forward modeling, point to electron scattering by TDSs as the primary driver of the observed low-energy precipitation and red-line diffuse-like auroras during this non-substorm event. Furthermore, during more active times like substorms, TDS wave amplitudes tend to intensify (Ergun et al., 2015; Shen et al., 2021; Khazanov et al., 2021). It remains to be determined how much TDSs contribute to the generation of red-line and green-line diffuse-like auroras during those active times.

5 Conclusion

This letter revisits a flow-related red-line aurora event initially reported by Liang et al. (2011). Analyzing THEMIS spectra and waveform measurements, we have revealed an abundance of time-domain structures (TDSs) associated with magnetotail flow bursts. Applying quasilinear calculations, we have estimated TDS-driven electron distributions precipitating into the ionosphere. Employing the time-dependent TREx-ATM auroral transport code, we have forward-modeled red-line auroras due to TDS-driven precipitation. The good correlation of $\sim$0.77 between modeled and observed red-line emissions suggests that TDSs likely cause the observed red-line diffuse-like auroras, which sometimes coexisted with or likely evolved from discrete forms. However, to fully explain the most intense red-line emissions, contributions from whistler-mode waves are also necessary. Our study suggests that wave-driven red-line diffuse-like auroras, associated with braking flow bursts, offer a distinct yet complementary pathway of MI-coupling compared with well-established flow-driven discrete auroral streamers, typically seen in the green line and caused by field-aligned potential acceleration.

Acknowledgments

This work has been supported by NASA projects 80NSSC23K0413, 80NSSC23K0108, 80NSSC22K1638, and 80NSSC20K1325. Q.M. acknowledges the NASA grant 80NSSC20K0196 and NSF grant AGS-2225445. L.L. acknowledges the NSF grant 2055192. J.L. acknowledges the NASA grants 80NSSC22K0749, 80NSSC22K0751, and NSF grant AGS-2247034. TREx-ATM is supported by Canadian Space Agency. We thank Jasper Laca for help with editing. We acknowledge the support of NASA contract NAS5-02099 for the use of data from the THEMIS Mission.

Open Research

THEMIS data is available at `http://themis.ssl.berkeley.edu/data/themis/`. Poker Flat DASC and MSP can be accessed at `http://optics.gi.alaska.edu/optics/?q=archive`. Data access and processing was done using SPEDAS V4.1, see Angelopoulos et al. (2019).

References

Agapitov, O. V., Artemyev, A., Krasnoselskikh, V., Khotyaintsev, Y. V., Mourenas, D., Breuillard, H., ... Rolland, G. (2013, June). Statistics of whistler mode waves in the outer radiation belt: Cluster STAFF-SA measurements. *J. Geophys. Res.*, *118*, 3407-3420. doi: 10.1002/jgra.50312

Angelopoulos, V. (2008, December). The THEMIS Mission. *Space Sci. Rev.*, *141*, 5-34. doi: 10.1007/s11214-008-9336-1

Angelopoulos, V., Baumjohann, W., Kennel, C. F., Coronti, F. V., Kivelson,

M. G., Pellat, R., ... Paschmann, G. (1992, April). Bursty bulk flows in the inner central plasma sheet. *J. Geophys. Res.*, *97*, 4027-4039. doi: 10.1029/91JA02701

Angelopoulos, V., Cruce, P., Drozdov, A., Grimes, E. W., Hatzigeorgiu, N., King, D. A., ... Schroeder, P. (2019, January). The Space Physics Environment Data Analysis System (SPEDAS). *Space Sci. Rev.*, *215*, 9. doi: 10.1007/s11214-018-0576-4

Angelopoulos, V., Sibeck, D., Carlson, C. W., McFadden, J. P., Larson, D., Lin, R. P., ... Sigwarth, J. (2008, December). First Results from the THEMIS Mission. *Space Sci. Rev.*, *141*, 453-476. doi: 10.1007/s11214-008-9378-4

Auster, H. U., Glassmeier, K. H., Magnes, W., Aydogar, O., Baumjohann, W., Constantinescu, D., ... Wiedemann, M. (2008, December). The THEMIS Fluxgate Magnetometer. *Space Sci. Rev.*, *141*, 235-264. doi: 10.1007/s11214-008-9365-9

Bonnell, J. W., Mozer, F. S., Delory, G. T., Hull, A. J., Ergun, R. E., Cully, C. M., ... Harvey, P. R. (2008, December). The Electric Field Instrument (EFI) for THEMIS. *Space Sci. Rev.*, *141*, 303-341. doi: 10.1007/s11214-008-9469-2

Cattell, C., Dombeck, J., Wygant, J., Drake, J. F., Swisdak, M., Goldstein, M. L., ... Balogh, A. (2005, January). Cluster observations of electron holes in association with magnetotail reconnection and comparison to simulations. *J. Geophys. Res.*, *110*, 1211. doi: 10.1029/2004JA010519

Chaston, C. C., Bonnell, J. W., Clausen, L., & Angelopoulos, V. (2012, September). Energy transport by kinetic-scale electromagnetic waves in fast plasma sheet flows. *J. Geophys. Res.*, *117*, 9202. doi: 10.1029/2012JA017863

Chaston, C. C., Peticolas, L. M., Bonnell, J. W., Carlson, C. W., Ergun, R. E., McFadden, J. P., & Strangeway, R. J. (2003, February). Width and brightness of auroral arcs driven by inertial Alfven waves. *Journal of Geophysical Research (Space Physics)*, *108*(A2), 1091. doi: 10.1029/2001JA007537

Cully, C. M., Ergun, R. E., Stevens, K., Nammari, A., & Westfall, J. (2008, December). The THEMIS Digital Fields Board. *Space Sci. Rev.*, *141*, 343-355. doi: 10.1007/s11214-008-9417-1

Damiano, P. A., Johnson, J. R., & Chaston, C. C. (2015, July). Ion temperature effects on magnetotail Alfvén wave propagation and electron energization. *J. Geophys. Res.*, *120*, 5623-5632. doi: 10.1002/2015JA021074

Donovan, E., Liu, W., Liang, J., Spanswick, E., Voronkov, I., Connors, M., ... Rae, I. J. (2008, August). Simultaneous THEMIS in situ and auroral observations of a small substorm. *Geophys. Res. Lett.*, *35*(17), L17S18. doi: 10.1029/2008GL033794

Ergun, R. E., Carlson, C. W., McFadden, J. P., Mozer, F. S., Delory, G. T., Peria, W., ... Kistler, L. (1998). FAST satellite observations of large-amplitude solitary structures. *Geophys. Res. Lett.*, *25*, 2041-2044. doi: 10.1029/98GL00636

Ergun, R. E., Goodrich, K. A., Stawarz, J. E., Andersson, L., & Angelopoulos, V. (2015, March). Large-amplitude electric fields associated with bursty bulk flow braking in the Earth's plasma sheet. *J. Geophys. Res.*, *120*, 1832-1844. doi: 10.1002/2014JA020165

Forsyth, C., Sergeev, V. A., Henderson, M. G., Nishimura, Y., & B., G. (2020). Physical Processes of Meso-Scale, Dynamic Auroral Forms. *Space Science Reviews*, *216*, 46. doi: 10.1007/s11214-020-00665-y

Franz, J. R., Kintner, P. M., Pickett, J. S., & Chen, L.-J. (2005, September). Properties of small-amplitude electron phase-space holes observed by Polar. *J. Geophys. Res.*, *110*, A09212. doi: 10.1029/2005JA011095

Gabrielse, C., Angelopoulos, V., Harris, C., Artemyev, A., Kepko, L., & Runov, A. (2017, May). Extensive electron transport and energization via multiple, localized dipolarizing flux bundles. *J. Geophys. Res.*, *122*, 5059-5076. doi: 10.1002/2017JA023981

Glauert, S. A., & Horne, R. B. (2005, April). Calculation of pitch angle and energy diffusion coefficients with the PADIE code. *J. Geophys. Res.*, *110*, 4206. doi: 10.1029/2004JA010851

Gurnett, D. A., & Frank, L. A. (1977, March). A region of intense plasma wave turbulence on auroral field lines. *J. Geophys. Res.*, *82*(7), 1031. doi: 10.1029/JA082i007p01031

Gurnett, D. A., Frank, L. A., & Lepping, R. P. (1976, December). Plasma waves in the distant magnetotail. *J. Geophys. Res.*, *81*, 6059-6071. doi: 10.1029/JA081i034p06059

Henderson, M. G. (2012). Auroral substorms, poleward boundary activations, auroral streamers, omega bands, and onset precursor activity. In *Auroral phenomenology and magnetospheric processes: Earth and other planets* (p. 39-54). American Geophysical Union (AGU). doi: https://doi.org/10.1029/2011GM001165

Henderson, M. G., Reeves, G. D., & Murphree, J. S. (1998). Are north-south aligned auroral structures an ionospheric manifestation of bursty bulk flows? *Geophysical Research Letters*, *25*(19), 3737-3740. Retrieved from `https://agupubs.onlinelibrary.wiley.com/doi/abs/10.1029/98GL02692` doi: https://doi.org/10.1029/98GL02692

Hull, A. J., Damiano, P. A., Chaston, C. C., Johnson, J. R., & Reeves, G. D. (2022, August). Electron Energization Signatures in Traveling Kinetic Alfvén Waves at Storm Time Injection Fronts. *Geophys. Res. Lett.*, *49*(15), e99318. doi: 10.1029/2022GL099318

Hutchinson, I. H. (2017, May). Electron holes in phase space: What they are and why they matter. *Physics of Plasmas*, *24*(5), 055601. doi: 10.1063/1.4976854

Kennel, C. F., & Engelmann, F. (1966, November). Velocity Space Diffusion from Weak Plasma Turbulence in a Magnetic Field. *Physics of Fluids*, *9*, 2377-2388. doi: 10.1063/1.1761629

Kennel, C. F., & Petschek, H. E. (1966, January). Limit on Stably Trapped Particle Fluxes. *J. Geophys. Res.*, *71*, 1-28.

Khazanov, G. V., Shen, Y., Vasko, I. Y., Artemyev, A. V., & Chu, M. (2021, May). Magnetosphere Ionosphere Coupling of Precipitated Electrons in Diffuse Aurora Driven by Time Domain Structures. *Geophys. Res. Lett.*, *48*(10), e92655. doi: 10.1029/2021GL092655

Le Contel, O., Roux, A., Robert, P., Coillot, C., Bouabdellah, A., de La Porte, B., ... Larson, D. (2008, December). First Results of the THEMIS Search Coil Magnetometers. *Space Sci. Rev.*, *141*, 509-534. doi: 10.1007/s11214-008-9371-y

Li, W., Bortnik, J., Thorne, R. M., & Angelopoulos, V. (2011, December). Global distribution of wave amplitudes and wave normal angles of chorus waves using THEMIS wave observations. *J. Geophys. Res.*, *116*, 12205. doi: 10.1029/2011JA017035

Liang, J., Donovan, E., Jackel, B., Spanswick, E., & Gillies, M. (2016, August). On the 630 nm red-line pulsating aurora: Red-line Emission Geospace Observatory observations and model simulations. *Journal of Geophysical Research (Space Physics)*, *121*(8), 7988-8012. doi: 10.1002/2016JA022901

Liang, J., Shen, Y., Knudsen, D., Spanswick, E., Burchill, J., & Donovan, E. (2019, June). e-POP and Red Line Optical Observations of Alfvénic Auroras. *Journal of Geophysical Research (Space Physics)*, *124*(6), 4672-4696. doi: 10.1029/2019JA026679

Liang, J., Spanswick, E., Nicolls, M. J., Donovan, E. F., Lummerzheim, D., & Liu, W. W. (2011, June). Multi-instrument observations of soft electron precipitation and its association with magnetospheric flows. *J. Geophys. Res.*, *116*, 6201. doi: 10.1029/2010JA015867

Lotekar, A., Vasko, I. Y., Mozer, F. S., Hutchinson, I., Artemyev, A. V., Bale, S. D.,

... Strangeway, R. (2020). Multisatellite mms analysis of electron holes in the earth's magnetotail: Origin, properties, velocity gap, and transverse instability. *Journal of Geophysical Research: Space Physics*, *125*(9), e2020JA028066. (e2020JA028066 10.1029/2020JA028066) doi: 10.1029/2020JA028066

Lyons, L. R. (1974, December). Pitch angle and energy diffusion coefficients from resonant interactions with ion-cyclotron and whistler waves. *Journal of Plasma Physics*, *12*, 417-432. doi: 10.1017/S002237780002537X

Lyons, L. R., Nishimura, Y., Gallardo-Lacourt, B., Nicolls, M. J., Chen, S., Hampton, D. L., ... Angelopoulos, V. (2015, June). Azimuthal flow bursts in the inner plasma sheet and possible connection with SAPS and plasma sheet earthward flow bursts. *Journal of Geophysical Research (Space Physics)*, *120*(6), 5009-5021. doi: 10.1002/2015JA021023

Lyons, L. R., Nishimura, Y., Xing, X., Runov, A., Angelopoulos, V., Donovan, E., & Kikuchi, T. (2012, February). Coupling of dipolarization front flow bursts to substorm expansion phase phenomena within the magnetosphere and ionosphere. *J. Geophys. Res.*, *117*, 2212. doi: 10.1029/2011JA017265

Lyons, L. R., Thorne, R. M., & Kennel, C. F. (1972). Pitch-angle diffusion of radiation belt electrons within the plasmasphere. *J. Geophys. Res.*, *77*, 3455-3474. doi: 10.1029/JA077i019p03455

Ma, Q., Connor, H. K., Zhang, X. J., Li, W., Shen, X. C., Gillespie, D., ... Spence, H. E. (2020, August). Global Survey of Plasma Sheet Electron Precipitation due to Whistler Mode Chorus Waves in Earth's Magnetosphere. *Geophys. Res. Lett.*, *47*(15), e88798. doi: 10.1029/2020GL088798

Ma, Q., Ni, B., Tao, X., & Thorne, R. M. (2012, April). Evolution of the plasma sheet electron pitch angle distribution by whistler-mode chorus waves in non-dipole magnetic fields. *Annales Geophysicae*, *30*, 751-760. doi: 10.5194/angeo-30-751-2012

Malaspina, D. M., Ukhorskiy, A., Chu, X., & Wygant, J. (2018, April). A Census of Plasma Waves and Structures Associated With an Injection Front in the Inner Magnetosphere. *J. Geophys. Res.*, *123*, 2566-2587. doi: 10.1002/2017JA025005

Malaspina, D. M., Wygant, J. R., Ergun, R. E., Reeves, G. D., Skoug, R. M., & Larsen, B. A. (2015). Electric field structures and waves at plasma boundaries in the inner magnetosphere. *J. Geophys. Res.*, *120*, n/a–n/a. (2015JA021137) doi: 10.1002/2015JA021137

Matsumoto, H., Kojima, H., Miyatake, T., Omura, Y., Okada, M., Nagano, I., & Tsutsui, M. (1994, December). Electrotastic Solitary Waves (ESW) in the magnetotail: BEN wave forms observed by GEOTAIL. *Geophys. Res. Lett.*, *21*, 2915-2918. doi: 10.1029/94GL01284

McFadden, J. P., Carlson, C. W., Larson, D., Ludlam, M., Abiad, R., Elliott, B., ... Angelopoulos, V. (2008, December). The THEMIS ESA Plasma Instrument and In-flight Calibration. *Space Sci. Rev.*, *141*, 277-302. doi: 10.1007/s11214-008-9440-2

Mende, S. B., Harris, S. E., Frey, H. U., Angelopoulos, V., Russell, C. T., Donovan, E., ... Peticolas, L. M. (2008, December). The THEMIS Array of Ground-based Observatories for the Study of Auroral Substorms. *Space Sci. Rev.*, *141*, 357-387. doi: 10.1007/s11214-008-9380-x

Meredith, N. P., Bortnik, J., Horne, R. B., Li, W., & Shen, X.-C. (2021). Statistical investigation of the frequency dependence of the chorus source mechanism of plasmaspheric hiss. *Geophysical Research Letters*, *48*(6), e2021GL092725. Retrieved from `https://agupubs.onlinelibrary.wiley.com/doi/abs/10.1029/2021GL092725` (e2021GL092725 2021GL092725) doi: https://doi.org/10.1029/2021GL092725

Mozer, F. S., Agapitov, O., Artemyev, A., Drake, J. F., Krasnoselskikh, V., Lejosne, S., & Vasko, I. (2015). Time domain structures: What and where they are,

what they do, and how they are made. *Geophys. Res. Lett.*, *42*, 3627-3638. doi: 10.1002/2015GL063946

Mozer, F. S., Agapitov, O. V., Hull, A., Lejosne, S., & Vasko, I. Y. (2018). Pulsating auroras produced by interactions of electrons and time domain structures. *J. Geophys. Res.*, *122*(8), 8604-8616. Retrieved from `https://agupubs.onlinelibrary.wiley.com/doi/abs/10.1002/2017JA024223` doi: 10.1002/2017JA024223

Muschietti, L., Ergun, R. E., Roth, I., & Carlson, C. W. (1999). Phase-space electron holes along magnetic field lines. *Geophys. Res. Lett.*, *26*, 1093-1096. doi: 10.1029/1999GL900207

Nakamura, R., Baumjohann, W., Schödel, R., Brittnacher, M., Sergeev, V. A., Kubyshkina, M., ... Liou, K. (2001, June). Earthward flow bursts, auroral streamers, and small expansions. *J. Geophys. Res.*, *106*(A6), 10791-10802. doi: 10.1029/2000JA000306

Newell, P. T., Sotirelis, T., & Wing, S. (2009, September). Diffuse, monoenergetic, and broadband aurora: The global precipitation budget. *J. Geophys. Res.*, *114*, A09207. doi: 10.1029/2009JA014326

Ni, B., Liang, J., Thorne, R. M., Angelopoulos, V., Horne, R. B., Kubyshkina, M., ... Lummerzheim, D. (2012, January). Efficient diffuse auroral electron scattering by electrostatic electron cyclotron harmonic waves in the outer magnetosphere: A detailed case study. *J. Geophys. Res.*, *117*, 1218. doi: 10.1029/2011JA017095

Ni, B., Thorne, R. M., Shprits, Y. Y., & Bortnik, J. (2008, June). Resonant scattering of plasma sheet electrons by whistler-mode chorus: Contribution to diffuse auroral precipitation. *Geophys. Res. Lett.*, *35*, 11106. doi: 10.1029/2008GL034032

Nishimura, Y., Bortnik, J., Li, W., Angelopoulos, V., Donovan, E. F., & Spanswick, E. L. (2018). Comment on "pulsating auroras produced by interactions of electrons and time domain structures" by mozer et al. *J. Geophys. Res.*, *123*(3), 2064-2070. Retrieved from `https://agupubs.onlinelibrary.wiley.com/doi/abs/10.1002/2017JA024844` doi: 10.1002/2017JA024844

Nishimura, Y., Lessard, M. R., Katoh, Y., Miyoshi, Y., Grono, E., Partamies, N., ... Kurita, S. (2020, January). Diffuse and Pulsating Aurora. *Space Sci. Rev.*, *216*(1), 4. doi: 10.1007/s11214-019-0629-3

Nishimura, Y., Lyons, L. R., Angelopoulos, V., Kikuchi, T., Zou, S., & Mende, S. B. (2011, September). Relations between multiple auroral streamers, pre-onset thin arc formation, and substorm auroral onset. *J. Geophys. Res.*, *116*, A09214. doi: 10.1029/2011JA016768

Scarf, F. L., Frank, L. A., Ackerson, K. L., & Lepping, R. P. (1974). Plasma wave turbulence at distant crossings of the plasma sheet boundaries and the neutral sheet. *Geophys. Res. Lett.*, *1*, 189-192. doi: 10.1029/GL001i005p00189

Sergeev, V. A., Angelopoulos, V., & Nakamura, R. (2012, March). Recent advances in understanding substorm dynamics. *Geophys. Res. Lett.*, *39*, 5101. doi: 10.1029/2012GL050859

Sergeev, V. A., Liou, K., Newell, P., Ohtani, S., Hairston, M., & Rich, F. (2004, February). Auroral streamers: characteristics of associated precipitation,convection and field-aligned currents. *Annales Geophysicae*, *22*, 537-548. doi: 10.5194/angeo-22-537-2004

Shen, Y., Artemyev, A., Zhang, X.-J., Vasko, I. Y., Runov, A., Angelopoulos, V., & Knudsen, D. (2020, August). Potential Evidence of Low-Energy Electron Scattering and Ionospheric Precipitation by Time Domain Structures. *Geophys. Res. Lett.*, *47*(16), e89138. doi: 10.1029/2020GL089138

Shen, Y., Artemyev, A. V., Zhang, X.-J., Zou, Y., Angelopoulos, V., Vasko, I., ... Wilkins, C. (2023, April). Contribution of Kinetic Alfvén Waves to Energetic Electron Precipitation From the Plasma Sheet During a Substorm. *Jour-*

nal of Geophysical Research (Space Physics), *128*(4), e2023JA031350. doi: 10.1029/2023JA031350

Shen, Y., Vasko, I. Y., Artemyev, A., Malaspina, D. M., Chu, X., Angelopoulos, V., & Zhang, X.-J. (2021, September). Realistic Electron Diffusion Rates and Lifetimes Due to Scattering by Electron Holes. *Journal of Geophysical Research (Space Physics)*, *126*(9), e29380. doi: 10.1029/2021JA029380

Solomon, S. C., Hays, P. B., & Abreu, V. J. (1988). The auroral 6300 a emission: Observations and modeling. *Journal of Geophysical Research: Space Physics*, *93*(A9), 9867-9882. doi: https://doi.org/10.1029/JA093iA09p09867

Tian, S., Colpitts, C. A., Wygant, J. R., Cattell, C. A., Ferradas, C. P., Igl, A. B., ... Donovan, E. F. (2021, May). Evidence of Alfvenic Poynting Flux as the Primary Driver of Auroral Motion During a Geomagnetic Substorm. *Journal of Geophysical Research (Space Physics)*, *126*(5), e29019. doi: 10.1029/2020JA029019

Tsyganenko, N. A. (1989, January). A magnetospheric magnetic field model with a warped tail current sheet. *Planetary Space Science*, *37*, 5-20. doi: 10.1016/0032-0633(89)90066-4

Vasko, I. Y., Agapitov, O. V., Mozer, F. S., Artemyev, A. V., Krasnoselskikh, V. V., & Bonnell, J. W. (2017, March). Diffusive scattering of electrons by electron holes around injection fronts. *J. Geophys. Res.*, *122*, 3163-3182. doi: 10.1002/2016JA023337

Vasko, I. Y., Krasnoselskikh, V. V., Mozer, F. S., & Artemyev, A. V. (2018, July). Scattering by the broadband electrostatic turbulence in the space plasma. *Physics of Plasmas*, *25*(7), 072903. doi: 10.1063/1.5039687

Williams, J. D., Chen, L. J., Kurth, W. S., Gurnett, D. A., & Dougherty, M. K. (2006, March). Electrostatic solitary structures observed at Saturn. *Geophys. Res. Lett.*, *33*(6), L06103. doi: 10.1029/2005GL024532

Yadav, S., Lyons, L. R., Liu, J., Nishimura, Y., Tian, S., Zou, Y., & Donovan, E. F. (2022). Association of equatorward extending auroral streamers with ground magnetic perturbations and geosynchronous injections. *Journal of Geophysical Research: Space Physics*, *127*(11), e2022JA030919. doi: https://doi.org/10.1029/2022JA030919

Zhang, X.-J., Angelopoulos, V., Ni, B., & Thorne, R. M. (2015, January). Predominance of ECH wave contribution to diffuse aurora in Earth's outer magnetosphere. *J. Geophys. Res.*, *120*, 295-309. doi: 10.1002/2014JA020455